



1 **Calibration methods for laser ablation Rb–Sr geochronology:**
2 **comparisons and recommendation based on NIST glass and**
3 **natural reference materials**

4 Stijn Glorie^{1*}, Sarah E. Gilbert², Martin Hand¹, Jarred C. Lloyd¹

5 ¹ *Department of Earth Sciences, University of Adelaide, SA 5005, Australia.*

6 ² *Adelaide Microscopy, University of Adelaide, SA 5005, Australia.*

7

8 *Correspondence to: Stijn Glorie (stijn.glorie@adelaide.edu.au)*

9

10 **Abstract**

11 In-situ Rb–Sr geochronology using LA-ICP-MS/MS technology allows rapid dating of K-rich
12 minerals such as micas (e.g. biotite, muscovite, phlogopite) and K-feldspar. While many studies
13 have demonstrated the ability of the method, analytical protocols vary significantly and to date no
14 studies have provided an in-depth comparison and synthesis in terms of precision and accuracy.
15 Here we compare four calibration protocols based on commonly used reference materials for Rb–
16 Sr dating. We demonstrate that downhole fractionation trends (DHF) for natural biotite, K-feldspar
17 and phlogopite contrast with that for the commonly used Mica-Mg nano-powder reference
18 material. Consequently, Rb–Sr dates calibrated to Mica-Mg can be up to 5% inaccurate and the
19 degree of inaccuracy appears to be unsystematic between analytical sessions. Calibrating to Mica-
20 Mg also introduces excess uncertainty that can be avoided with a more consistent primary
21 calibration material. We propose a calibration approach involving NIST-610 glass as the primary



22 reference material (RM) and a natural mineral with similar DHF characteristics to the analysed
23 samples as secondary RM to correct for matrix-dependent fractionation. In this work, MDC
24 phlogopite (the source mineral for Mica-Mg nano-powder) was used as the secondary RM,
25 consistently producing accurate Rb–Sr dates for a series of natural biotites and K-feldspars with
26 well-characterized expected ages. However, biotite from the Banalasta Adamellite, Taratap
27 Granodiorite and Entire Creek pegmatite are also suitable secondary RMs for Rb/Sr ratio
28 calibration purposes with consistently <1.5% fully propagated uncertainties in our methodological
29 approach. Until calibration using isochronous natural standards as the primary RM becomes
30 possible in data-reduction software, the two-step calibration approach described here is
31 recommended.

32

33 **Keywords:** reaction-cell ICP-MS; in-situ geochronology; Rb–Sr reference materials; calibration
34 standards

35

36 1. Introduction

37 Rubidium-Strontium (Rb–Sr) geochronology using laser ablation – inductively coupled plasma –
38 tandem mass spectrometry (LA-ICP-MS/MS) has become a popular method to constrain the
39 formation or cooling age of potassium-bearing minerals (Gorojovsky and Alard, 2020; Hogmalm
40 et al., 2017; Jegal et al., 2022; Kirkland et al., 2023; Larson et al., 2023; Laureijs et al., 2021; Li
41 et al., 2020; Liebmann et al., 2022; Olierook et al., 2020; Redaa et al., 2021; Rosel and Zack, 2022;
42 Sengun et al., 2019; Tillberg et al., 2021; Tillberg et al., 2020; Wang et al., 2022; Zack and
43 Hogmalm, 2016). In contrast to traditional Rb–Sr dating involving column-chemistry in



44 specialized laboratories, the laser-ablation method allows rapid acquisition of Rb–Sr dates directly
45 from thin sections or rock blocks with minimal sample preparation. The method involves the use
46 of an ICP-MS/MS, equipped with a reaction cell where isobaric isotopes can be chemically
47 separated due to their significant differences in reactivity with an introduced reaction gas (Balcaen
48 et al., 2015 and references therein). Applied to Rb–Sr geochronology, CH₃F, SF₆, O₂ and N₂O
49 have been used as reaction gasses (e.g. Hogmalm et al., 2017; Moens et al., 2001; Zack and
50 Hogmalm, 2016), with the latter being the most widely used for quadrupole ICP-MS/MS due to
51 its high reactivity. However, published analytical methodologies for LA-ICP-MS/MS Rb–Sr
52 dating vary significantly beyond the applied reaction gas (Table 1). Reported laser conditions
53 (fluence and repetition rate) are largely laser-wavelength dependent with common conditions
54 being either $\sim 5 - 7 \text{ J.cm}^{-2} / 10 \text{ Hz}$ for 213nm lasers, especially during initial development work
55 (e.g. Hogmalm et al., 2017; Laureijs et al., 2021; Rosel and Zack, 2022; Sengun et al., 2019;
56 Tillberg et al., 2020; Zack and Hogmalm, 2016) or $\sim 2 - 4 \text{ J.cm}^{-2} / 5 \text{ Hz}$ for 193nm lasers (e.g.
57 Kirkland et al., 2023; Larson et al., 2023; Li et al., 2020; Liebmann et al., 2022; Olierook et al.,
58 2020; Redaa et al., 2021). The applied calibration protocols for mass discrimination and elemental
59 fractionation, however, vary more significantly. Most published work uses a glass reference
60 material (RM), with NIST-610 being most popular to correct for drift and calibrate the Sr isotopic
61 ratios. Rb/Sr ratios are most commonly calibrated against Mica-Mg, a phlogopite prepared as a
62 pressed nano-powder pellet, regardless of the analysed mineral (micas in most published work).
63 However, the approach varies, with some methods directly calibrating to Mica-Mg as the primary
64 RM (e.g. Gorojovsky and Alard, 2020; Hogmalm et al., 2017; Li et al., 2020; Redaa et al., 2021;
65 Rosel and Zack, 2022; Sengun et al., 2019; Wang et al., 2022) and others using NIST-610 as the
66 primary RM followed by a correction for matrix-dependent fractionation against Mica-Mg as



67 secondary RM (e.g. Liebmann et al., 2022; Olierook et al., 2020). Other secondary RMs, used to
68 verify the accuracy of obtained dates, are either glass reference materials (e.g. Larson et al., 2023;
69 Laureijs et al., 2021; Rosel and Zack, 2022) or in-house natural materials such as the La Posta
70 biotite (Zack and Hogmalm, 2016), the MDC phlogopite (Redaa et al., 2021), or the CK001 biotite
71 (Olierook et al., 2020).

72 In addition, laser-induced down-hole fractionation (DHF) can occur during ablation and aerosol
73 condensation processes and is most apparent when ratioing elements with contrasting volatilities
74 (e.g. Jackson and Günther, 2003; Košler et al., 2005; Longerich et al., 1996). Elemental Sr is more
75 refractory than the volatile Rb and hence has a high potential to fractionate during laser ablation
76 (Zack and Hogmalm, 2016). A small number of studies have directly compared different
77 calibration approaches and have described differences in Rb–Sr DHF behaviour between
78 commonly used reference materials (e.g. Redaa et al., 2021; Wang et al., 2022). However,
79 systematic comparisons between data reduction protocols, tested with natural materials, are limited
80 in the current literature. Here, we compare four different calibration approaches for a series of
81 natural biotite and K-feldspar samples. The samples were taken from quickly cooled igneous rocks,
82 eliminating potential diffusion-related issues when comparing dates of different minerals. Hence,
83 the well-constrained igneous crystallization ages are the expected reference ages for the analysed
84 samples and one of the biotite samples has previously been dated by the Rb–Sr ID-TIMS method.
85 The calibration approaches we compare are:

86 (A) NIST-610 as the primary RM for both $^{87}\text{Rb}/^{87}\text{Sr}$ and $^{87}\text{Sr}/^{86}\text{Sr}$ ratios plus MDC phlogopite as
87 secondary RM to correct for matrix-dependant fractionation;

88 (B) NIST-610 as the primary RM for both $^{87}\text{Rb}/^{87}\text{Sr}$ and $^{87}\text{Sr}/^{86}\text{Sr}$ ratios plus Mica-Mg pressed
89 pellet as secondary RM to correct for matrix-dependant fractionation;



90 (C) Mica-Mg as the primary RM for $^{87}\text{Rb}/^{87}\text{Sr}$ ratios and NIST-610 as the primary RM for
91 $^{87}\text{Sr}/^{86}\text{Sr}$ ratios;

92 (D) Mica-Mg as the primary RM for both $^{87}\text{Rb}/^{87}\text{Sr}$ and $^{87}\text{Sr}/^{86}\text{Sr}$ ratios

93 We discuss the differences between these approaches in terms of accuracy and precision, and
94 highlight the importance of monitoring and correcting down-hole fractionation with appropriate
95 reference materials.

96

97 **2. Sample descriptions**

98 **2.1. MDC phlogopite and Mica-Mg nano powder**

99 Mica-Mg nano-powder is used as a reference material for Rb–Sr dating. It consists of crushed
100 phlogopite from Bekily (Madagascar) with a high Rb ($1300 \pm 40 \mu\text{g.g}^{-1}$) and low Sr ($27 \pm 3 \mu\text{g.g}^{-1}$)
101 concentration (Redaa et al., 2023 and references therein). MDC is natural phlogopite, which was
102 sourced from the same locality as Mica-Mg (Redaa et al., 2021). The reference age for both
103 materials is 519.4 ± 6.5 Ma and the initial $^{87}\text{Sr}/^{86}\text{Sr}$ ratio is 0.72607 ± 0.0007 , constrained from a
104 diopside (low-Rb mineral) that occurs in the same location (Hogmalm et al., 2017). However, for
105 Mica-Mg some pellet to pellet variation in both Rb/Sr and Sr/Sr ratios has been observed (Jegal et
106 al., 2022; Redaa et al., 2023).

107 **2.2. Entire Creek pegmatite**

108 The Entire Creek sample was taken from a deformed pegmatite in the Harts Range meta-igneous
109 complex of central Australia, in the same location as described by Mortimer et al. (1987). The
110 pegmatite cross-cuts folded and foliated amphibolites, is composed of coarse-grained quartz,



111 plagioclase, alkali feldspar and biotite, with the latter defining a strong axial-plane foliation to
112 folds outlined by the pegmatite. Biotite and whole-rock Rb/Sr and Sr/Sr isotope ratios, obtained
113 by ID-TIMS at the University of Adelaide, are reported in Mortimer et al. (1987) and define a 7-
114 point (3 biotite and 4 whole rock analyses) isochron age of $312.1 \pm 1.8 / 5.1$ Ma (95% confidence
115 uncertainties, without / with overdispersion), recalculated in IsoplotR (Vermeesch, 2018), using
116 the Villa et al. (2015) Rb–Sr decay constant of $1.3972 \pm 0.0045 \times 10^{-11} \text{ a}^{-1}$ (Appendix 1).

117 **2.3. Banalasta Adamellite (Bundarra Suite)**

118 The S-type Banalasta Adamellite forms the southern end the Bundarra Batholith in the Southern
119 New England Orogen in eastern Australia (e.g. Flood and Shaw, 1975; Jeon et al., 2012;
120 Rosenbaum et al., 2012; Shaw and Flood, 1981). The Bundarra Batholith is an elongate north-
121 south trending magmatic suite, spanning approximately 200 km. The Banalasta Adamellite is
122 approximately 40 km in diameter and has sharp contacts with surrounding metasediments with a
123 contact metamorphic aureole characterised by fine-grained cordierite-bearing assemblage at the
124 pluton margin grading out to regional prehnite-pumpellyite metagreywacke assemblages over a
125 distance of approximately 3 km (Flood and Shaw, 1977). Internally the granite is massive, coarse-
126 grained granitoid containing approximately equal proportions of K-feldspar and plagioclase,
127 together with accessory apatite, zircon and monazite. Biotite predominantly occurs in multi-grain
128 clots together with quartz, plagioclase, magnetite, zircon and apatite. In rare cases they contain
129 relic garnet, suggesting they formed from hydration of garnet entrained from the granitic source
130 region.

131 Melt-precipitated zircon from the Banalasta Adamellite gives zircon U-Pb ages of 286.2 ± 2.2 Ma
132 (Black, 2007), 289.2 ± 1.7 Ma (Jeon et al., 2012) and 282 ± 4 Ma (Phillips et al., 2011). Whole
133 rock Rb–Sr data from the Bundarra Suite gives an age of 285 ± 15 Ma ($n = 6/7$, MSWD = 0.4).



134 When additional feldspar Rb–Sr data are included in the isochron, the isochron age is 283 ± 10 Ma
135 ($n = 9/10$, MSWD = 0.24) (Appendix 2). Both isochron dates were recalculated using the data from
136 Flood and Shaw (1977) and the decay constant from Villa et al. (2015). Additionally, Hensel et al
137 (1995) reported a model whole rock Rb–Sr age of 287 ± 10 Ma for a group of 16 samples from the
138 Bundarra Suite. Overall, it is evident that Rb–Sr age data is similar to the ages of melt precipitated
139 zircon, consistent with the lack of evidence for extended fractional crystallisation (Jeon et al 2012).
140 The samples used in this study come from the same location as Black (2007) that has a granitic
141 zircon of 286.2 ± 2.2 Ma, as well as a second location approximately 800 meters away.

142

143 **2.4. Taratap Granodiorite**

144 The Taratap Granodiorite in the Delamerian Orogenic belt in southern Australia is classified as S-
145 type, calc-alkaline with a composition dominated by microcline megacrysts (c. 3–4 cm in length),
146 which define a NNE-trending magmatic fabric in a coarse-grained groundmass of plagioclase,
147 quartz, K-feldspar and biotite, with accessory zircon, apatite, and monazite. Low-temperature
148 alteration is evident in thin section by the presence of chlorite–muscovite–titanite and minor
149 allanite (Burt and Abbot, 1998). The sample was chosen for analysis because the timing of
150 emplacement is tightly constrained by a zircon U–Pb ID-TIMS age of 497.11 ± 0.56 Ma ($^{206}\text{Pb}/^{238}\text{U}$
151 weighted mean age, 95% confidence interval uncertainty, MSWD = 1.8, $n = 6$) and an apatite Lu-
152 Hf age of 497.1 ± 5.5 Ma (MSWD = 1.1, $n = 38$) (Glorie et al., 2023 and references therein).

153

154 **3. Analytical methods**



155 All Rb–Sr analyses were conducted at Adelaide Microscopy, University of Adelaide, using an
156 Agilent 8900x ICP-MS/MS, coupled to a RESolution-LR ArF excimer (193 nm) laser ablation
157 system. A squid mixing device (Laurin Technic) was used to smooth the pulsed laser signal
158 between the laser and the mass-spectrometer. The instrument parameters follow those reported in
159 Redaa et al. (2021), with ablation in a He atmosphere ($350 \text{ mL}\cdot\text{min}^{-1}$), mixed with Ar ($890 \text{ mL}\cdot\text{min}^{-1}$)
160 as the carrier gas and N_2 ($3.5 \text{ mL}\cdot\text{min}^{-1}$) added before the ICP torch to enhance the signal
161 sensitivity. N_2O ($0.37 \text{ mL}\cdot\text{min}^{-1}$) was used as the reaction gas to separate ^{87}Sr from ^{87}Rb . The ^{86}Sr
162 and ^{87}Sr isotopes were measured as their oxide reaction products (e.g. $^{87}\text{Sr}^{16}\text{O}$) with a mass shift
163 of 16 amu between the two quadrupole mass analysers (e.g. $Q1 = 87 \text{ m/z}$, $Q2 = 103 \text{ m/z}$). Despite
164 the high reaction efficiency of ^{87}Sr , residual unreacted Sr prevents direct measurement of ^{87}Rb .
165 Instead, ^{85}Rb was measured as a proxy for ^{87}Rb and calculated assuming natural isotopic
166 abundance. The samples and reference materials were ablated using a circular laser beam of 67
167 μm diameter, a fluence of $3.5 \text{ J}\cdot\text{cm}^{-2}$, and repetition rate of 5 Hz . Further details are presented in
168 Table 2. A total of three analytical sessions were conducted, with largely identical instrumental
169 parameters between the different sessions. The ICP-MS was tuned to a sensitivity which kept Rb
170 in pulse mode in Mica-Mg (the material with the highest Rb concentration), negating the
171 requirement for additional pulse-analogue (P/A) corrections.
172 For each analytical session, NIST-610, Mica-Mg and MDC were used as reference materials for
173 calibration purposes. All data was processed in LADR (Norris and Danyushevsky, 2018) using a
174 customized data reduction algorithm that calculates error correlations from the raw isotopic ratios
175 for each sweep in an analysis, in the same way as for U-Pb data reduction. Isotope ratios were
176 calculated by: (1) correcting down-hole fractionation (DHF) against the primary RM, (2) averaging



177 the DHF corrected ratios of each sweep in the analysis, and then (3) normalising to a the primary
178 RM to correct for matrix independent instrument mass bias and drift.

179 Normalisation of the measured Rb/Sr and Sr/Sr ratios was conducted with two different reference
180 materials (NIST-610 and Mica-Mg), following the four analytical protocols outlined above (A-D).

181 The reference $^{87}\text{Rb}/^{87}\text{Sr}$ and $^{86}\text{Sr}/^{87}\text{Sr}$ ratios used for Mica-Mg were 83.4 ± 1.0 and $0.53981 \pm$
182 0.00070 , respectively (Hogmalm et al., 2017). For NIST-610, the $^{87}\text{Rb}/^{87}\text{Sr}$ was calculated from

183 ppm data as 3.28 ± 0.03 and for the $^{86}\text{Sr}/^{87}\text{Sr}$ ratio, the reference value of 1.409048 ± 0.000036
184 was used (Woodhead and Hergt, 2001). For each normalization protocol, DHF corrections of the

185 Rb–Sr ratios were applied based on the DHF behaviour of the applied primary RM. No DHF
186 correction was applied to the $^{86}\text{Sr}/^{87}\text{Sr}$ ratios. Where NIST-610 was used as the primary RM, MDC

187 phlogopite or Mica-Mg were used as secondary RM to correct the $^{87}\text{Rb}/^{87}\text{Sr}$ ratios for matrix-
188 dependant fractionation (cfr. Roberts et al., 2017 for U/Pb ratios; Simpson et al., 2022 for Lu/Hf

189 ratios).

190 All mica samples (including biotite samples and MDC phlogopite) were ablated with the laser
191 ablating parallel to cleavage. The Bundarra samples were analysed in thin section and the Taratap

192 sample as a rock block. The coarse Entire Creek biotites were mounted as mica-books using a vice
193 to prevent air-gaps between individual mica sheets, with the ‘pages’ of the book mounted upright

194 exposing multiple cleavage planes perpendicular to the surface.

195 For each sample and reference material, inverse isochron Rb–Sr dates (Li and Vermeesch, 2021)
196 were calculated in IsoplotR (Vermeesch, 2018), based on the processed $^{87}\text{Rb}/^{87}\text{Sr}$ and $^{86}\text{Sr}/^{87}\text{Sr}$

197 ratios, their 2SE uncertainties, and the calculated error correlations. Reported inverse isochron
198 uncertainties are fully propagated 95% confidence intervals, including the uncertainty on the decay

199 constant and added uncertainty for overdispersion where required (calculated in IsoplotR). The



200 exceptions are the inverse isochron dates for MDC and Mica-Mg when used as secondary RMs,
201 which are used to correct the Rb/Sr ratios when calibrating to NIST-610. For these cases the
202 reported uncertainties are 95% confidence uncertainties without external uncertainties (as the
203 external uncertainties would otherwise be applied twice to the isochron dates of the analysed
204 samples). Session-dependant correction factors (CF) were calculated from the measured $^{87}\text{Rb}/^{87}\text{Sr}$
205 ratio for MDC and Mica-Mg and compared to the reference value (calculated from the published
206 age for both MDC and Mica-Mg of 519.4 ± 6.5 Ma; Hogmalm et al., 2017; Redaa et al., 2021).
207 These CF values (= measured ratio/expected ratio) were subsequently applied to each unknown
208 analysis when calibrated to either MDC or Mica-Mg. Finally, the uncertainties on the MDC and
209 Mica-Mg dates are propagated to the reported Rb–Sr isochron uncertainties for each NIST-610
210 calibrated sample using the quadratic addition of the relative uncertainties.

211

212 **4. Results**

213 **4.1. Downhole fractionation trends**

214 In this section, we compare the downhole fractionation (DHF) trend of the $^{87}\text{Rb}/^{87}\text{Sr}$ ratio between
215 the analysed feldspars and micas and the reference materials (NIST-610 and Mica-Mg) (Fig. 1).
216 The obtained fractionation trends do not vary significantly between different sessions; however,
217 data from analytical session 3 is presented as it contains data for all analysed samples presented in
218 this paper. The DHF trends were calculated in LADR and individual scatter plots can be found in
219 Appendix 3. As shown, The DHF trends for the analysed biotite, phlogopite and K-feldspar
220 samples are internally consistent, showing ~10% increase in Rb/Sr ratio over the first 20 s of
221 ablation, followed by a flatter trend in the subsequent 20 s. NIST-610 shows a similar trend of
222 increasing Rb/Sr ratio with ablation time, however the amplitude of the DHF curve is more



223 subdued compared to the natural samples (~3.5% increase in the first 20 s ablation). In contrast,
224 the DHF pattern for Mica-Mg shows an oscillating trend, increasing for the first ~10 s of ablation
225 and then dropping for the subsequent ~30 s of ablation (Fig. 1).

226

227 **4.2. Within-session reproducibility of $^{87}\text{Rb}/^{87}\text{Sr}$ and $^{86}\text{Sr}/^{87}\text{Sr}$ ratios**

228 Figure 2 shows the within-session variability of the $^{87}\text{Rb}/^{87}\text{Sr}$ and $^{86}\text{Sr}/^{87}\text{Sr}$ ratios for both primary
229 RMs NIST-610 and Mica-Mg in analytical session 3. The reference materials are considered
230 homogenous in both isotopic ratios, meaning that any variations are purely due to differences in
231 the ablation characteristics from spot to spot. As shown, the measured $^{87}\text{Rb}/^{87}\text{Sr}$ ratios and $^{86}\text{Sr}/^{87}\text{Sr}$
232 ratios are significantly more consistent for NIST-610 compared to Mica-Mg (both measured using
233 the same analytical conditions and spot size). The maximum within-session variability (=min-max
234 range) in the $^{87}\text{Rb}/^{87}\text{Sr}$ ratio is < 3% for NIST-610, compared to > 8% for Mica-Mg. The $^{86}\text{Sr}/^{87}\text{Sr}$
235 ratio is more consistent for both primary RMs, however, the uncertainty on individual analyses is
236 approximately 3× larger for Mica-Mg compared to NIST-610. ICP-MS mass-bias drift is minimal
237 for both isotope ratios in NIST-610, with only a slight increase in the Rb/Sr ratio over the first 2-
238 3 hours of analysis. As both Mica-Mg and NIST-610 were analysed sequentially in the same
239 analytical session, the apparent ‘drift’ in the Mica-Mg $^{86}\text{Sr}/^{87}\text{Sr}$ ratios are due to variations in
240 ablation rather than changes in the ICP-MS mass bias.

241 **4.3. Isochron Rb–Sr dates for natural K-feldspars and micas**

242 Inverse isochron plots and resulting Rb–Sr dates are presented for each analytical protocol in
243 Appendix 4. Summary plots are shown in Figure 3. The data-table with the input $^{87}\text{Rb}/^{87}\text{Sr}$ and
244 $^{86}\text{Sr}/^{87}\text{Sr}$ ratios is accessible from Figshare via the link in the data availability section. For the



245 Bundarra samples, the biotite isochrons are anchored to apatite Rb/Sr ratios, given that the apatites
246 commonly occur as inclusions within biotite. For the K-feldspars, the isochrons are anchored to
247 plagioclase, given that the analysed K-feldspars often show minor exsolution with plagioclase.
248 However, the choice of anchoring mineral gives no difference in the obtained biotite and K-
249 feldspar inverse isochron Rb/Sr dates. For the Taratap sample, isochron anchoring was conducted
250 to a combination of plagioclase and apatite in session 1, but only plagioclase in sessions 2 and 3,
251 given the limited occurrence of apatite in thin section. For the Entire Creek biotite sample,
252 anchoring was conducted to whole-rock $^{86}\text{Sr}/^{87}\text{Sr}$ ratios from Mortimer et al. (1987). The MDC
253 and Mica-Mg isochrons were anchored to an initial $^{86}\text{Sr}/^{87}\text{Sr}$ ratio of 1.3773 ± 0.0013 and
254 calibrated to the published age of 519.4 ± 6.5 Ma (Hogmalm et al., 2017; Redaa et al., 2021).

255 The summary of obtained inverse Rb–Sr dates is presented in Table 3. As shown, there is only
256 marginal variation in the absolute biotite dates between the three analytical protocols involving
257 Mica-Mg, either as the primary RM for Rb/Sr ratios (protocols C & D) or as a secondary RM
258 (protocol B). Hence, in order to evaluate the accuracy of the obtained Rb–Sr dates against the
259 expected references ages for each sample, we only compare the first two analytical protocols
260 (NIST-610 as the primary RM and either: (A) MDC or (B) Mica-Mg as secondary RM).

261 Figure 4 compares the obtained Rb–Sr inverse isochron dates to the expected ages for the three
262 samples, that were analysed over two or three analytical sessions. The uncertainties for the K-
263 feldspar dates are not shown as they are too large to be useful (due to the relatively low radiogenic
264 nature of typical K-feldspar versus micas), here we only compare the accuracy of the absolute
265 dates. As shown, analytical protocol (A) involving NIST as primary RM and MDC phlogopite as
266 secondary RM consistently gives the most accurate Rb–Sr dates across all different analytical
267 sessions. For this analytical protocol, the Rb–Sr biotite dates for the Bundarra samples are 287.1



268 ± 2.4 Ma, 284.7 ± 3.0 Ma, 287.7 ± 2.3 Ma and 285.7 ± 2.6 Ma (between two samples over two
269 analytical sessions), which are in excellent agreement with the published zircon U-Pb age of 286.2
270 ± 2.2 Ma (Black, 2007) from the same outcrop. The K-felspar dates of 290 ± 14 Ma, 285 ± 15 Ma,
271 290 ± 37 Ma and 288 ± 37 Ma are in excellent agreement as well but are less useful to evaluate
272 age accuracies given their larger uncertainties. Similarly for the Taratap sample, the obtained
273 biotite Rb–Sr dates of 499.4 ± 3.6 Ma and 495.7 ± 4.0 Ma as well as the (imprecise) K-feldspar
274 Rb–Sr dates of 500 ± 30 Ma, 501 ± 50 Ma and 495 ± 35 Ma are in excellent agreement with the
275 zircon U-Pb ID-TIMS age of 497.1 ± 0.6 Ma as well as the apatite Lu-Hf age of 497.1 ± 5.5 Ma
276 for the same sample (Glorie et al., 2023). Hence, the combined dataset suggests that the biotite, K-
277 feldspar and zircons record the same (crystallization) age for both the Bundarra and Taratap
278 samples. The Entire Creek biotite gave consistent Rb–Sr dates of 310.7 ± 1.5 Ma and 311.6 ± 3.1
279 Ma, in excellent agreement with the ID-TIMS age of $312.1 \pm 1.8 / 5.1$ Ma (95% confidence
280 uncertainties, without / with overdispersion), based on the Rb/Sr ratios in Mortimer et al. (1987),
281 recalculated with the Villa et al. (2015) Rb–Sr decay constant.

282 **5. Discussion**

283 **5.1. Downhole fractionation corrections**

284 Few previous studies have reported Rb–Sr DHF trends for a series of artificial reference materials
285 (i.e. glass standards and pressed pellets; Redaa et al., 2021; Wang et al., 2022). However, to the
286 best of our knowledge, DHF trends have not been evaluated for natural materials with the
287 exception of phlogopite MDC (Redaa et al., 2021). In our experiments, DHF is more pronounced
288 in natural micas and K-feldspar than observed for the NIST-610 glass and Mica-Mg pressed pellet,
289 when ablated under the same analytical conditions (Fig. 1). Comparatively, Mica-Mg appears least
290 appropriate to correct the analysed samples for DHF, given its systematically different DHF trend.



291 NIST-610 shows less DHF compared to the analysed micas and K-feldspars but its trend is more
292 systematic (similar shape with lower amplitudes). Thus, correcting for DHF against NIST-610
293 reduces the observed DHF for the analysed samples, while Mica-Mg significantly under-corrects
294 for DHF or accentuates it when applied to minerals. MDC biotite would be the most appropriate
295 choice for DHF correction as it behaves very similar to the analysed mica and K-feldspar samples.
296 However, as with most natural materials, MDC is not sufficiently homogenous in $^{87}\text{Rb}/^{87}\text{Sr}$ ratio
297 to be used as a primary RM. While the shape or slope of DHF trends can vary depending on laser
298 conditions (spot size, frequency and fluence), it cannot be eliminated for elements with contrasting
299 volatilities such as Rb and Sr. However, based on the presented data, the use of NIST-610 is the
300 more appropriate reference material to correct for DHF and Mica-Mg would exacerbate instead of
301 reduce the effects of DHF.

302 If no DHF correction is applied, accurate data can only be achieved if exactly the same signal
303 interval is selected in both the secondary RM and sample. If there is a residual DHF slope on the
304 sample Rb/Sr ratios that is different to the RM (e.g. crystalline material versus Mica-Mg), then
305 selecting a shorter signal interval can significantly bias Rb/Sr ratios and hence the apparent age.

306

307 **5.2. Mica-Mg vs NIST-610 and MDC as calibration standards**

308 **5.2.1. Uncertainty comparisons**

309 The contributions to the propagated uncertainties of individual analyses from the reference
310 materials (average signal precision and calibration curve misfit) are much larger when calibrating
311 to Mica-Mg compared to NIST-610 for both $^{87}\text{Rb}/^{87}\text{Sr}$ and $^{86}\text{Sr}/^{87}\text{Sr}$ ratios (Fig. 5). For example,
312 in analytical session 1, the obtained uncertainties for individual $^{87}\text{Rb}/^{87}\text{Sr}$ ratios for the Entire
313 Creek biotite sample are more than double when using Mica-Mg compared to NIST-610 as the



314 primary RM (Fig. 5; Appendix 5). As a result, the choice of Mica-Mg instead of NIST-610 as the
315 primary RM might mask the presence of multiple data populations and introduces excessive
316 uncertainties onto isochron dates.

317 The use of Mica-Mg as calibration standard for $^{86}\text{Sr}/^{87}\text{Sr}$ ratios most significantly affects the
318 isochron precision of low-radiogenic samples such as K-feldspar samples. As shown in Table 3
319 and Figure 5, the uncertainty on the K-feldspar isochron dates can be up to $2\times$ larger, compared to
320 other calibration methods. Furthermore, the resulting MSWD values on the isochron regressions
321 are consistently < 0.3 (Table 3), suggesting excessive uncertainties on individual data-points. For
322 the more radiogenic biotite samples, the larger uncertainties in $^{86}\text{Sr}/^{87}\text{Sr}$ ratios have negligible
323 effects to the precision on the isochron dates.

324 The precision of the calibrated $^{87}\text{Rb}/^{87}\text{Sr}$ ratios is more important to the isochron uncertainty of
325 highly radiogenic materials, such as most types of micas. Calibrating to NIST-610 versus Mica-
326 Mg yields either more precise biotite isochron dates or identical precision. However, when NIST-
327 610 is used as the primary RM, propagation of the uncertainty on MDC or Mica-Mg to the resulting
328 isochron age uncertainty is either identical or slightly worse compared to using Mica-Mg as
329 calibration standard (Fig. 5; Table 3). The difference relates to the degree of overdispersion. The
330 larger uncertainties on the Rb/Sr ratios when using Mica-Mg as primary RM result in lower
331 MSWD values, reducing the uncertainty on the isochron regression. This excess uncertainty when
332 calibrating to Mica-Mg might mask meaningful geological scatter in Rb/Sr ratios and it is therefore
333 advisable to produce isochrons based on data with the best possible analytical precision.

334 In summary, Mica-Mg should not be used as calibration standard for $^{86}\text{Sr}/^{87}\text{Sr}$ ratio calculations
335 for low-radiogenic samples as it introduces excessive uncertainties to age calculations. For high-
336 radiogenic samples, using Mica-Mg as the primary RM also introduces larger uncertainties to



337 individual data-points compared to using NIST-610, but there is no significant difference in
338 propagated uncertainty after secondary correction to either MDC or Mica-Mg. For Rb/Sr ratio
339 calibrations, NIST-610 is more consistent, resulting in lower uncertainties on individual Rb/Sr
340 ratios. When there is no overdispersion, this results in better isochron age precision. However,
341 overdispersion can be masked by the increased uncertainties on Rb/Sr ratios, resulting in better
342 apparent precision when data is calibrated to Mica-Mg.

343 **5.2.2. Accuracy comparisons**

344 It has been observed previously that Rb–Sr dates are offset from their expected ages when
345 calibrated to the NIST-610 reference material (e.g. Gorojovsky and Alard, 2020; Wang et al.,
346 2022). In contrast, Mica-Mg seems to better reproduce expected ages, although the significant
347 uncertainties obtained for natural materials in previous studies render appropriate accuracy testing
348 difficult. For example, Wang et al. (2022) compares measured to expected Rb–Sr dates for three
349 samples with known ages. The best achieved uncertainty in their experiment was ~2.6% for one
350 sample, while for the other samples the reported uncertainties are ~5.6 and 6.3 %. Similarly, the
351 accuracy comparisons in Gorojovsky and Alard (2020) use the Monastery phlogopite, with a
352 precision of ~4% when calibrated to Mica-Mg. Both papers report data normalized to NIST-610
353 but do not apply a secondary correction for matrix-dependent fractionation.

354 For the biotites analysed in our study, the fully propagated 95% confidence interval uncertainties
355 ranges between 0.8 and 1.6% when calibrated to Mica-Mg and between 1.0% and 1.4% when
356 calibrated to NIST-610 and corrected to MDC (depending on the sample and analytical session;
357 Table 3), allowing for more detailed accuracy comparisons. Figure 4 illustrates that using NIST-
358 610 and MDC as calibration reference materials produces the most accurate results, compared to
359 the expected references dates. For the biotite results, the obtained Rb–Sr dates are within 0.5%



360 accuracy compared to the expected ages. The K-feldspar dates are accurate within 1%, except for
361 session 2, where accuracy is within 1.5%. When the same data is calibrated against Mica-Mg
362 (either using NIST-610 as the primary RM and Mica-Mg as secondary RM, or directly using Mica-
363 Mg as the primary RM), the results are significantly offset from their expected ages. For the biotite
364 results calibrated to Mica-Mg, accuracy is within 2% for sessions 2 and 3 and there is 5% age off-
365 set in session 1. For the K-feldspars, the age offset is up to 2.5% in sessions 2 and 3 and 6% in
366 session 1. While the age offsets in sessions 2 and 3 might be regarded as 'acceptable', given the
367 obtained precision, the more significant inaccuracy in session 1 renders Mica-Mg to be less
368 desirable as a primary RM.

369 The difference in accuracy between session 1 and sessions 2 and 3 can be explained by the
370 difference in measured dates for the MDC and Mica-Mg reference materials, normalised to NIST-
371 610. For sessions 2 and 3, MDC and Mica-Mg produced similar isochron dates (2.3 and 1.9%
372 difference respectively) (Table 3; Fig. 6). For session 1, however, MDC gives a significantly
373 different age (494 ± 4 Ma) compared to Mica-Mg (469 ± 4 Ma). These differences in accuracy (ca.
374 5 % in session 1 and ca. 2 % in sessions 2 and 3) are in line with the observed age off-sets between
375 the measured dates and reference dates for the biotite and K-feldspar samples, calibrated to Mica-
376 Mg.

377

378 **5.2.3. Long-term comparison between MDC and Mica-Mg as secondary calibration** 379 **standards**

380 Given that the accuracy of the Rb–Sr method appears to be significantly dependent on the applied
381 calibration reference materials, and that the measured Rb–Sr dates of these calibration standards
382 fluctuate significantly between analytical sessions when compared to NIST-610, the long-term



383 behaviour of the MDC and Mica-Mg reference materials needs to be evaluated. Figure 7 presents
384 2.5 years of measured Rb–Sr dates for MDC and Mica-Mg, both calibrated to NIST-610 as the
385 primary RM. All data in this plot have been processed identically. The Rb–Sr dates for Mica-Mg
386 are generally more consistent, ranging between ca. 462 and 479 Ma, with a standard deviation of
387 4.5 Ma, while the MDC dates show more variation, ranging between ca. 465 and 494 Ma, with a
388 standard deviation of 7.7 Ma. In all but two sessions, MDC produces an older Rb–Sr date compared
389 to Mica-Mg. The analytical sessions discussed above are highlighted in Figure F and encompass
390 the maximum variability in measured Rb–Sr dates for MDC. With the premise that calibration to
391 NIST-610 and MDC produces accurate Rb–Sr dates (as discussed in section 5.2.2), the difference
392 between the measured MDC and Mica-Mg dates (Fig. 6, 7) can be regarded as an estimate of the
393 degree of inaccuracy when data is calibrated to Mica-Mg. While some sessions reveal very little
394 off-set between both standards, using Mica-Mg as calibration standard can lead to up to 5%
395 inaccuracy in Rb–Sr dates. The cause of the observed variability is currently unknown, however,
396 in the second-to-last session with a significantly older Mica-Mg date compared to MDC, the
397 analysed samples might have received a lower effective laser fluence compared to other sessions
398 as the glass between the laser beam and samples was not cleaned prior to analysis. The lower
399 fluence could change the effective matrix bias between NIST-610, Mica-Mg and MDC, however,
400 calibration of biotite against MDC produces accurate results as demonstrated in section 5.2.2. In
401 contrast, although Mica-Mg produces more consistent Rb–Sr dates between analytical sessions,
402 these dates are unreliable given the variable and unsystematic degree of inaccuracy between
403 sessions.

404

405 **6. Conclusions**



406 Based on our observations, the use of Mica-Mg as calibration reference material is not
407 recommended, for the following reasons:

408 (1) The down-hole fractionation (DHF) trend for Mica-Mg is not comparable with the DHF
409 trends of natural biotite, phlogopite and K-feldspar (Fig. 1). Using Mica-Mg to correct DHF
410 would exacerbate instead of reduce DHF in those minerals;

411 (2) Given the relatively poor reproducibility of $^{87}\text{Rb}/^{87}\text{Sr}$ ratios and significant uncertainty on
412 individual $^{87}\text{Sr}/^{86}\text{Sr}$ measurements (Fig. 2), Mica-Mg as primary RM or secondary RM
413 introduces excess uncertainty that can be avoided using a more consistent primary RM such as
414 NIST-610;

415 (3) We demonstrated that calibrating to Mica-Mg may lead to up to 5% inaccuracy in Rb–Sr
416 age (Fig. 4, 6, 7) and that the degree of inaccuracy is unsystematically session-dependant.

417 We suggest a different approach, involving (1) calibration of the $^{87}\text{Rb}/^{87}\text{Sr}$ and $^{87}\text{Sr}/^{86}\text{Sr}$ ratios to a
418 primary reference material with high Rb and Sr concentrations and homogenous isotopic ratios
419 such as NIST-610 glass, including DHF correction of the Rb/Sr ratios, followed by (2) a correction
420 of the $^{87}\text{Rb}/^{87}\text{Sr}$ ratio to a natural mineral secondary RM with a similar DHF trend as the samples
421 to be analysed. In our observations, there are no significant differences in matrix effects comparing
422 biotite, phlogopite and K-feldspar, suggesting that any of these natural minerals as secondary RM
423 can produce accurate dates for K-rich minerals. We have used MDC phlogopite as secondary RM
424 and demonstrate accurate Rb–Sr dates for a range of biotites and K-feldspars with well-established
425 age constraints. The fully propagated uncertainties for the analysed biotites are <1.5%, allowing
426 accuracy verifications at high analytical precision.



427 Finally, while this two-step calibration protocol is currently recommended due to current
428 constraints with data processing software, new developments involving calibrating to isochronous
429 reference materials might become the desired approach in the future.

430

431 **Data availability**

432 The Rb–Sr dataset used in this manuscript is freely available on figshare at
433 <https://doi.org/10.25909/23996484>.

434

435

436 **Acknowledgements**

437 This paper was supported by research grant FT210100906 and DP220103037 from the Australian
438 Research Council (ARC).

439

440

441 **Author contributions**

442 SG: Conceptualization, investigation, writing – original draft, methodology, funding acquisition,
443 visualisation, formal analysis

444 SEG: Conceptualization, investigation, writing – review and editing, methodology

445 MH: Conceptualization, investigation, writing - review and editing, resources

446 JCL: Conceptualization, investigation, writing - review and editing, formal analysis

447

448 **Competing interests**

449 The authors declare that they have no conflict of interest.

450

451 **Ethical statement**

452 This manuscript is an original work that is not submitted or published elsewhere.

453



454 Tables

	React. gas (ml.min ⁻¹)	Laser wavel. (nm)	Fluence (J.cm ⁻²)	Rep. rate (Hz)	Spot (μm)	Rb-Sr calibration	Sr-Sr calibration	DHF	Err. corr.
Zack and Hogmalm 2016	O ₂ (0.25)	213	7	10	80	Pl: NIST 610; Ksp: BCR-2G; Bt: La Posta	NIST 610	No	No
Hogmalm et al. 2017	O ₂ (0.25) N ₂ O (0.16) SF ₆ (0.04)	213	O ₂ : 7 N ₂ O: 6-8 SF ₆ : 6-8	10 4-5 10	80 50 50	Mica-Mg	NIST 610	No	No
Tillberg et al. 2020	N ₂ O (?)	213	?	?	50	BCR-2G (Sec: Mica-Mg/La Posta)	NIST 610	No	Yes
Rösel and Zack 2022	N ₂ O (0.18-0.20)	213	5-7	10	50-60	Mica-Mg (sec: NIST 610 / BCR-2G)	Mica-Mg	No	No
Gorojovsky and Alard 2020	N ₂ O (0.25)	193 and 213	7.8	5	85	Mica-Mg	Mica-Mg, NIST 610, BHVO-2G	No	No?
Larson et al 2023	N ₂ O (0.37)	193	4	10	50	Mica-Mg (Sec: Mica-Fe)	NIST 610	Yes?	Yes
Laureijs et al. 2021	CH ₃ F (10%)	213	6	10	50	ATHO-G, T1-G, StHs6/80-G	NIST 612	No	Yes
Li et al. 2020	N ₂ O (0.35)	193	3.5	5	74	Mica-Mg Sec: MDC	Mica-Mg	No	No
Liebmann et al. 2022	N ₂ O (?)	193	2.5	5	64	NIST-610 + Mica-Mg Sec: CK001 bt	NIST-610	No	Yes (est)
Olierook et al. 2020	N ₂ O (0.25)	193	2.5	5	64-87	NIST-610 + Mica-Mg Sec: CK001 bt	NIST-610	No	No
Redaa et al. 2021	N ₂ O (0.37)	193	3.5	5	74	Mica-Mg Sec: MDC	Mica-Mg	monitored	No
Sengun et al. 2019	N ₂ O (?)	213	5.7	10	50	Mica-Mg	NIST 610	No	No
Tilberg et al. 2021	N ₂ O (?)	213	?	?	50	Mica-Mg / NIST 610	NIST 610	No	Yes
Wang et al. 2022	N ₂ O (0.25)	193	7	5	85	Mica-Mg	NIST 610, BHVO-2G, BCR-2G	monitored	No
Kirkland et al. 2023	N ₂ O (0.25)	193	2	5	64	Mica-Mg Sec: CK001 bt	NIST 610	No	No



455 **Table 1:** Summary of published analytical conditions and protocols for LA-ICP-MS/MS Rb–Sr
456 dating. Rep. rate = laser repetition rate; Sec = secondary reference material; Bt = biotite; ksp = K-
457 feldspar; Pl = plagioclase; Err. Corr. = error correlation calculated; est = estimated formula. In case
458 of method development work - `best conditions` are quoted.

459



Analytical conditions

Plasma Settings	
RF power	1350 W
Sample Depth	5.0 mm
Ar carrier gas	0.89 L/min
He carrier gas	0.38 L/min
N ₂ addition	4 mL/min
Lens Parameters	
Extract 1	1.5 V
Extract 2	-80 V
Omega Bias	-85 V
Omega Lens	5.0 V
Q1 entrance	-10 V
Q1 exit	-2.0 V
Cell focus	-2.0 V
Cell Entrance	-90 V
Cell Exit	-120 V
Deflect	10 V
Plate Bias	-80 V
Q1 bias	-2.0 V
Q1 Prefilter Bias	-10.0 V
Q1 Postfilter Bias	-10.0 V
N ₂ O gas flow	0.37 mL/min
Octopole bias	-6.0 V
Axial Acceleration	2.0 V
Octopole RF	180 V
Energy Discrimination	-7.0 V
Analysis Parameters	
Laser Wavelength	193 nm
Laser fluence	3.5 J/m ²
Sample laser diameter	67 μm
Laser repetition rate	5 Hz
Background	30 s
Analysis time	40 s
Isotopes measured & dwell times (ms)	²³ Na (2), ²⁴ Mg (2), ²⁷ Al (2), ²⁹⁺¹⁶ Si (2), ³¹⁺¹⁶ P (2), ³⁹ K (2), ⁴³⁺¹⁶ Ca (2), ⁵⁵ Mn (2), ⁵⁶⁺¹⁶ Fe (2), ⁸⁵ Rb (10), ⁸⁶⁺¹⁶ Sr (50), ⁸⁷⁺¹⁶ Sr (50), ⁸⁸⁺¹⁶ Sr (50), ⁸⁹⁺¹⁶ Y (5), ⁹⁰⁺³² Zr (5), ⁹³⁺³² Nb (5), all x+16REE (5), ²³²⁺¹⁵ Th (5), ²³⁸⁺¹⁶ U (5)

460
461

462 **Table 2:** Analytical conditions for the three LA-ICP-MS/MS sessions in this paper.



Sample (exp. age)	S	n	(A) NIST + MDC		(B) NIST + Mica-Mg		(C) Mica-Mg & NIST		(D) Mica-Mg	
			Age ($\pm 2\sigma$) [Ma]	MS WD	Age ($\pm 2\sigma$) [Ma]	MS WD	Age ($\pm 2\sigma$) [Ma]	MS WD	Age ($\pm 2\sigma$) [Ma]	MS WD
Ent Crk Bt (312.1 \pm 1.8 ¹)	1	24	310.7 \pm 1.5/2.5/3.1	1.1	327.8 \pm 1.7/2.7/3.2	0.96	327.6 \pm 3.3/3.9	0.27	328.8 \pm 3.4/4.0	0.25
	3	20	311.6 \pm 3.1/3.8/4.5	2.5	317.6 \pm 3.2/3.8/4.6	2.4	316.1 \pm 3.2/3.8	0.85	316.2 \pm 3.2/3.8	0.84
Bund1b Bt (286.2 \pm 2.2 ²)	2	44	287.1 \pm 1.6/2.4/3.4	1.6	280.3 \pm 1.5/2.4/3.2	1.7	280.1 \pm 1.6/2.4	0.97	280.2 \pm 1.6/2.4	0.82
	3	22	284.7 \pm 2.4/3.0/3.8	1.0	290.1 \pm 2.5/3.1/3.8	1.1	288.4 \pm 4.1/4.5	0.7	288.2 \pm 4.3/4.7	0.28
Bund1b Ksp (286.2 \pm 2.2 ²)	2	57	290 \pm 14/14/14	0.87	284 \pm 14/14/14	0.88	284 \pm 14/14	0.84	280 \pm 23/23	0.3
	3	53	287 \pm 15/15/15	0.88	292 \pm 15/15/15	0.88	290 \pm 15/16	0.86	283.4 \pm 38/38	0.19
Bund6a Bt (286.2 \pm 2.2 ²)	2	38	287.7 \pm 1.3/2.3/3.4	1.4	280.9 \pm 1.3/2.2/3.1	1.5	279.5 \pm 1.5/2.3	0.71	279.5 \pm 1.5/2.3	0.7
	3	22	285.7 \pm 1.9/2.6/3.4	0.74	291.2 \pm 1.9/2.7/3.6	0.72	288.7 \pm 3.5/4.0	0.54	288.8 \pm 3.6/4.0	0.34
Bund6a Ksp (286.2 \pm 2.2 ²)	2	45	290 \pm 37/37/37	0.69	283 \pm 36/36/36	0.69	281 \pm 36/36	0.68	283 \pm 75/75	0.16
	3	40	288 \pm 37/37/37	0.65	293 \pm 38/38/38	0.65	294 \pm 39/39	0.65	296 \pm 93/93	0.11
Taratap Bt (497.1 \pm 0.6 ³)	2	30	499.4 \pm 1.8/3.6/5.6	1.2	487.7 \pm 1.7/3.5/5.2	1.2	489.6 \pm 2.8/4.2	0.67	489.6 \pm 2.8/4.2	0.63
	3	16	495.7 \pm 2.5/4.0/5.5	1.2	505.1 \pm 2.6/4.1/5.8	1.2	504.0 \pm 5.4/6.3	0.51	504.0 \pm 5.5/6.3	0.52
Taratap Ksp (497.1 \pm 0.6 ³)	1	54	500 \pm 30/30/30	0.53	527 \pm 31/31/31	0.53	527 \pm 32/32	0.50	539 \pm 58/58	0.14
	2	20	501 \pm 50/50/50	0.58	490 \pm 49/49/49	0.58	492 \pm 50/50	0.56	494 \pm 106/106	0.12
	3	18	495 \pm 35/35/35	0.95	504 \pm 36/36/36	0.95	490 \pm 39/39	1.1	511 \pm 63	0.3

463

464

Secondary RM	S	n	NIST-610 as primary RM	
			Age ($\pm 2\sigma$) [Ma]	MS WD
MDC	1	34	494.4 \pm 3.0	1.4
	2	21	464.5 \pm 4.0	1.3
	3	30	470.6 \pm 3.6	1.1
MicaMG	1	35	468.6 \pm 2.5	2.8
	2	21	475.7 \pm 3.7	3.5
	3	20	461.8 \pm 3.7	2.7

465

466



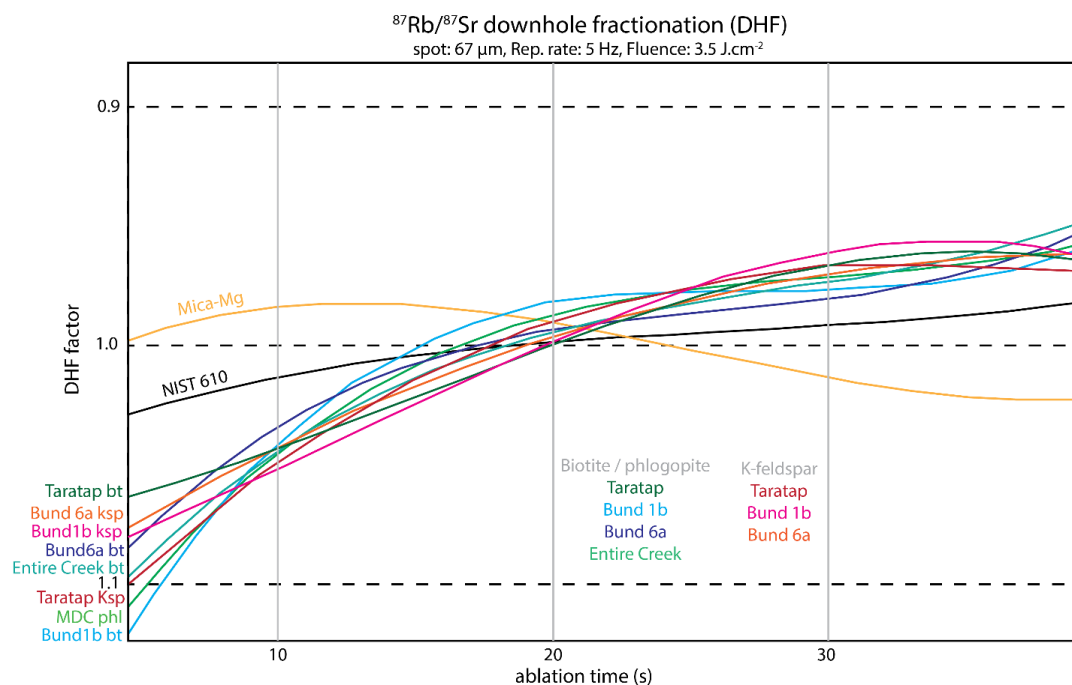
467 **Table 3:** Summary table of Rb–Sr dates obtained in this study. S = session number, n = number of analysed grains, exp. age = expected
468 reference age (see below). All uncertainties are 95% confidence intervals and are reported as (1) excluding external uncertainty (on the
469 decay constant) / (2) including external uncertainties / (3) with propagated uncertainty from the correction standard (for methods (A)
470 and (B) only). (A) NIST-610 as primary RM and MDC as secondary RM to calibrate Rb/Sr ratios; (B) NIST-610 as primary RM, Mica-
471 MG as secondary RM to calibrate Rb/Sr ratios; (C) Rb/Sr ratios calibrated to Mica-MG as primary RM and Sr/Sr ratios calibrated to
472 NIST-610 as secondary RM; (D) Mica-MG as primary RM for both Rb/Sr and Sr/Sr ratios. ¹ Rb-Sr TIMS age from Mortimer et al.
473 (1987), recalculated with Villa et al. (2015) decay constant in IsoplotR (Vermeesch, 2018). The reported uncertainty is 95% confidence
474 interval but does not take overdispersion into account. ² Zircon U-Pb age for the Banalasta Adamellite in the Bundarra Suite, from Black
475 (2007). ³ Zircon U-Pb TIMS age for the Taratap Granodiorite, reported in Glorie et al. (2023).

476



477 **Figure Captions**

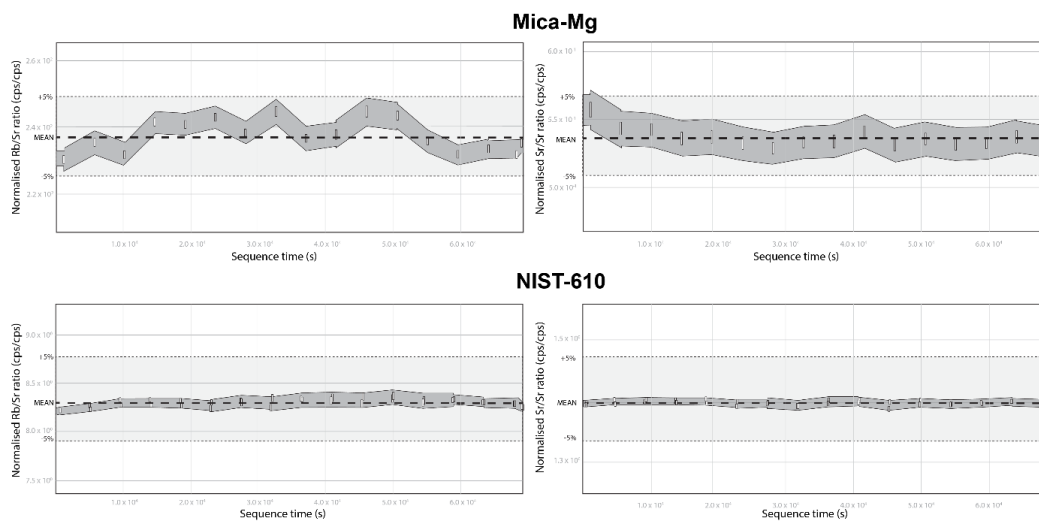
478



479

480 **Figure 1:** $^{87}\text{Rb}/^{87}\text{Sr}$ downhole fractionation profiles for the analysed reference materials Mica-Mg
481 (yellow line) and NIST-610 (black line), the biotite / phlogopite (green-blue lines) and K-feldspar
482 (red-pink lines) samples in analytical session 3, calculated in LADR (Norris and Danyushevsky,
483 2018). The DHF factor is calculated relative to the average ratio of the ablation signal (i.e. DHF
484 factor of 1 = average $^{87}\text{Rb}/^{87}\text{Sr}$ ratio of the downhole signal).

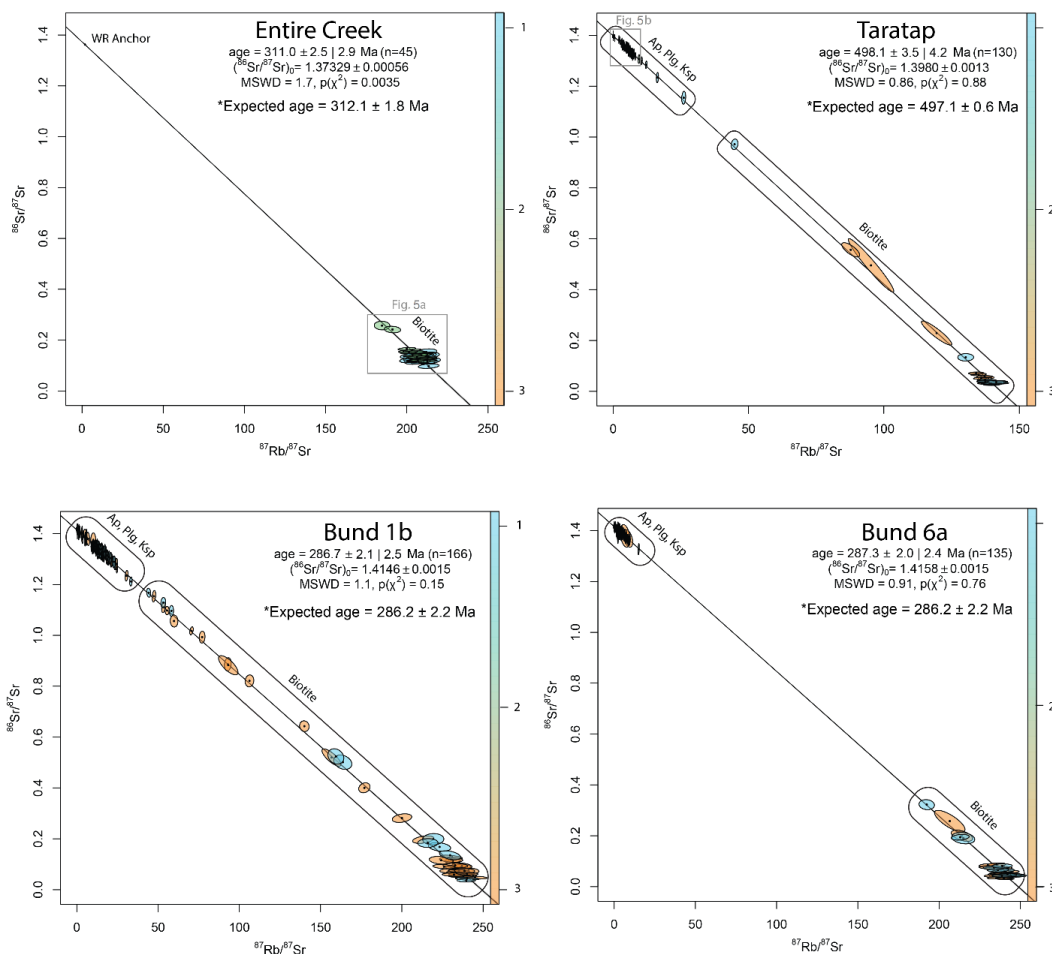
485



486

487 **Figure 2:** Variability of the $^{87}\text{Rb}/^{87}\text{Sr}$ and $^{86}\text{Sr}/^{87}\text{Sr}$ ratios for the analysed reference materials
488 NIST-610 and Mica-Mg over the total duration of analytical session 3. All plots are scaled equally
489 to $\pm 5\%$ variation of the mean to aid visual comparisons. The vertical bars are ± 1 standard
490 deviation. The gray envelopes models ± 2 standard deviation (note that for NIST-610 each standard
491 was measured twice at each standard bracket).

492



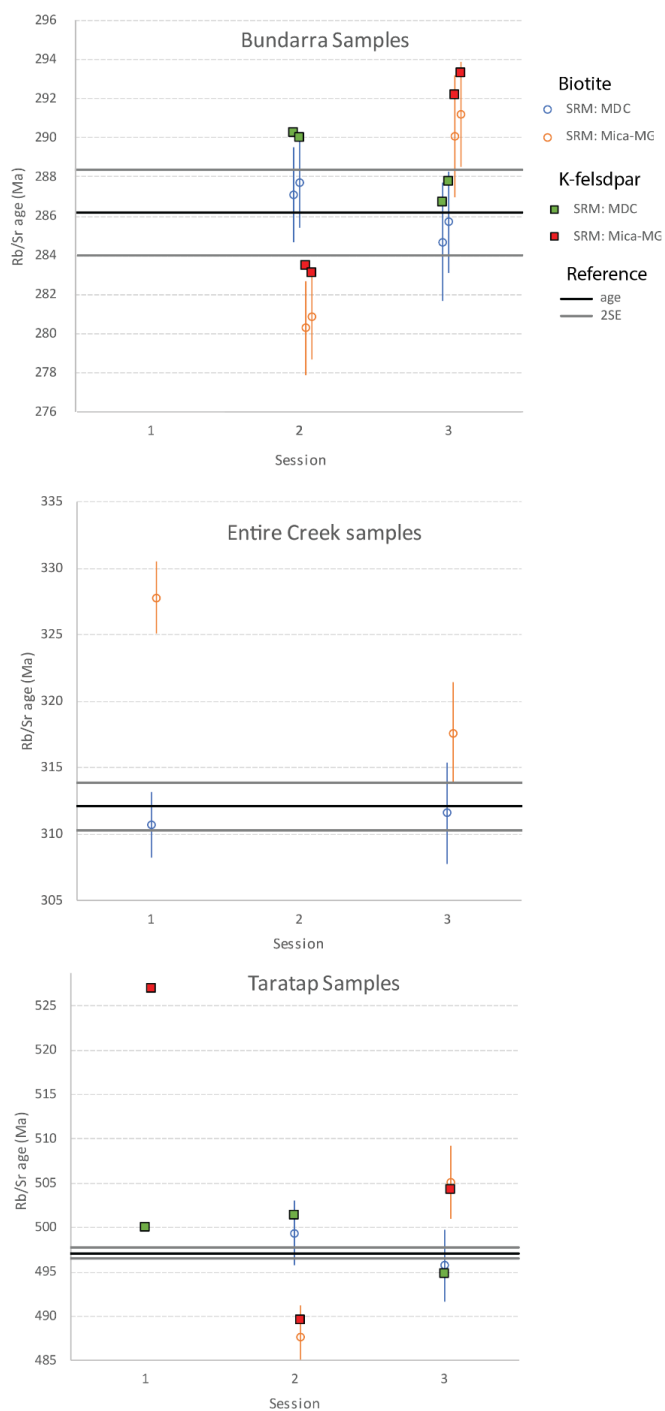
493

494 **Figure 3:** Pooled multi-mineral Rb–Sr isochron dates for the Entire Creek, Taratap and the two
495 Bundarra samples (Bund 1b and Bund 6a). The data was calibrated against NIST-610 as primary
496 RM and MDC as secondary RM (see text for details). The colour-code refers to the analytical
497 session in which the data was obtained. Biotite analyses plot towards the radiogenic lower-
498 intercept of the inverse isochrons, while feldspar and apatite anchor Rb/Sr ratios plot towards the
499 low-radiogenic end of the isochron regression. All plots were calculated in IsoplotR (Vermeesch,
500 2018), reporting 95% confidence interval uncertainties (including the uncertainty on the decay-
501 constant) with and without propagated uncertainty from the MDC secondary RM. Expected ages



502 are the recalculated Rb–Sr age from Mortimer et al. (1987) with the Villa et al. (2015) decay
503 constant for the Entire Creek sample; the zircon U-Pb ID-TIMS age reported in Glorie et al. (2023)
504 for the Taratap sample, and the Zircon SHRIMP U-Pb age from Black (2007) for the Bundarra
505 samples (see text for further details).

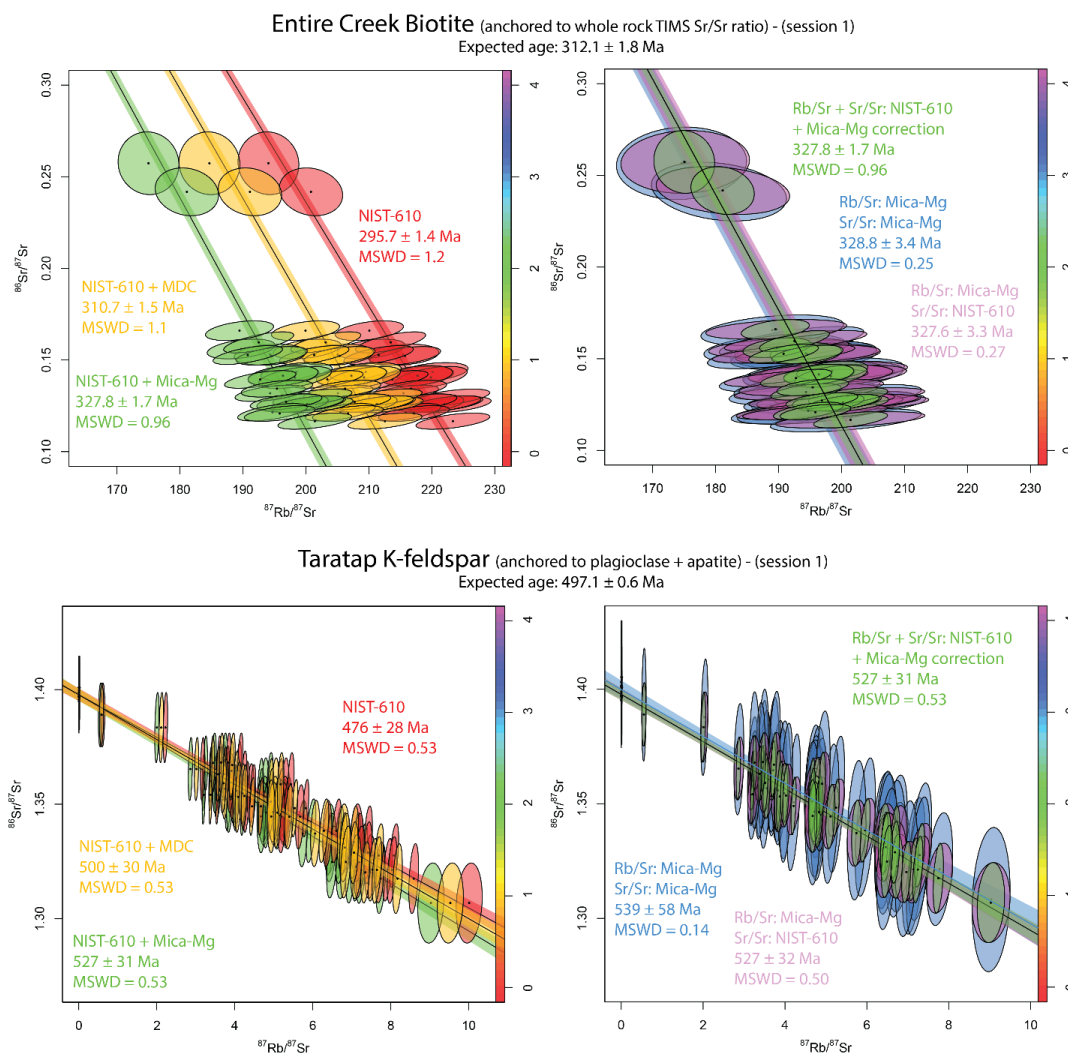
506





508 **Figure 4:** Comparisons of Rb–Sr dates over three analytical sessions, calibrated to either MDC or
509 Mica-Mg as secondary RM, with respect to the expected ages for each sample (black line with
510 gray 2SE uncertainty bars). In all cases, NIST-610 was used as primary RM. Biotite data are
511 plotted as open circles (blue = calibrated to MDC as secondary RM, orange = calibrated to Mica-
512 Mg as secondary RM). K-feldspar data are plotted as filled squares (green = calibrated to MDC as
513 secondary RM, red = calibrated to Mica-Mg as secondary RM).

514

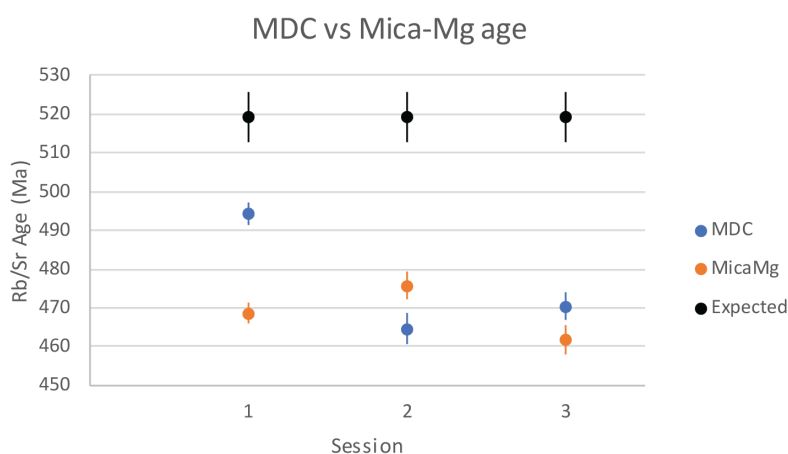


515

516 **Figure 5:** Comparisons of isochron dates obtained using the 4 different calibration protocols using
 517 the session 1 biotite Rb–Sr data from the Entire Creek sample and K-feldspar Rb–Sr data from the
 518 Taratap sample. Data plotted in red = NIST-610 as primary RM without correction for matrix-
 519 induced fractionation. Data plotted in green = NIST-610 as primary RM with Mica-Mg as
 520 secondary RM. Data plotted in yellow = NIST-610 as primary RM with MDC as secondary RM.
 521 Data plotted in purple = NIST-610 as primary RM for Sr/Sr ratios and Mica-Mg as primary RM



522 for Rb/Sr ratios. Data plotted in blue = both Rb/Sr and Sr/Sr ratios calibrated to Mica-Mg as
523 primary RM. The biotite data are highly radiogenic and show significant age differences depending
524 on the used secondary RM. The K-feldspar data are low radiogenic, resulting in larger and
525 overlapping uncertainties (refer to Figure 3 for full isochron plots). Using NIST-610 as primary
526 RM produces the smallest uncertainties on individual data-points.
527



528
529 **Figure 6:** Rb–Sr dates for MDC and Mica-Mg calibrated to NIST-610 over the three analytical
530 sessions used in this paper. The off-set of the Rb–Sr age with respect to the reference age is used
531 to calculate the correction factor on the Rb/Sr ratios.
532



533

534 **Figure 7:** Long-term (2.5 years) Rb–Sr age data for Mica-Mg and MDC for the lab (Adelaide
535 Microscopy). The top plot shows absolute dates and the bottom plot shows the percentage
536 difference between the MDC and Mica-Mg dates. All data were processed in the same way using
537 NIST-610 as primary RM. The three analytical sessions previously discussed are highlighted by
538 black rims and capture the most extreme differences obtained in our lab to date. Given that MDC
539 as secondary RM produces consistently accurate data, the plot indicates that Mica-Mg as primary
540 RM can lead to up to 5% inaccuracy in Rb–Sr age calculations.



541

542 References

- 543 Balcaen, L., Bolea-Fernandez, E., Resano, M., Vanhaecke, F., 2015. Inductively coupled plasma – Tandem
544 mass spectrometry (ICP-MS/MS): A powerful and universal tool for the interference-free
545 determination of (ultra)trace elements – A tutorial review. *Analytica Chimica Acta*, 894: 7-19.
- 546 Black, L., 2007. SHRIMP U–Pb zircon ages obtained during 2006/07 for NSW Geological Survey projects.
- 547 Burt, A.C., Abbot, P.J., 1998. The Taratap Granodioritite, South-East South Australia. *MESA Journal*, 10:
548 35-39.
- 549 Flood, R.H., Shaw, S.E., 1975. A cordierite-bearing granite suite from the New England Batholith, N.S.W.,
550 Australia. *Contributions to Mineralogy and Petrology*, 52(3): 157-164.
- 551 Flood, R.H., Shaw, S.E., 1977. Two “S-type” granite suites with low initial $^{87}\text{Sr}/^{86}\text{Sr}$ ratios from the New
552 England Batholith, Australia. *Contributions to Mineralogy and Petrology*, 61(2): 163-173.
- 553 Glorie, S. et al., 2023. Robust laser ablation Lu-Hf dating of apatite: an empirical evaluation. *Geological*
554 *Society of London Special Publication*, In press.
- 555 Gorojovsky, L., Alard, O., 2020. Optimisation of laser and mass spectrometer parameters for their
556 situ analysis of Rb/Sr ratios by LA-ICP-MS/MS. *JOURNAL OF ANALYTICAL ATOMIC SPECTROMETRY*,
557 35(10): 2322-2336.
- 558 Hogmalm, K.J., Zack, T., Karlsson, A.K.O., Sjöqvist, A.S.L., Garbe-Schonberg, D., 2017. In situ Rb-Sr and K-
559 Ca dating by LA-ICP-MS/MS: an evaluation of N_2O and SF_6 as reaction gases. *Journal of Analytical*
560 *Atomic Spectrometry*, 32(2): 305-313.
- 561 Jackson, S.E., Günther, D., 2003. The nature and sources of laser induced isotopic fractionation in laser
562 ablation-multicollector-inductively coupled plasma-mass spectrometry. *Journal of Analytical*
563 *Atomic Spectrometry*, 18(3): 205-212.
- 564 Jégou, Y. et al., 2022. Characterisation of Reference Materials for In Situ Rb-Sr Dating by LA-ICP-MS/MS.
565 *Geostandards and Geoanalytical Research*, 46(4): 645-671.
- 566 Jeon, H., Williams, I.S., Chappell, B.W., 2012. Magma to mud to magma: Rapid crustal recycling by Permian
567 granite magmatism near the eastern Gondwana margin. *Earth and Planetary Science Letters*, 319-
568 320: 104-117.
- 569 Kirkland, C.L. et al., 2023. Dating mylonitic overprinting of ancient rocks. *Communications Earth &*
570 *Environment*, 4(1): 47.
- 571 Košler, J. et al., 2005. Chemical and phase composition of particles produced by laser ablation of silicate
572 glass and zircon—implications for elemental fractionation during ICP-MS analysis. *Journal of*
573 *Analytical Atomic Spectrometry*, 20(5): 402-409.
- 574 Larson, K.P., Button, M., Shrestha, S., Camacho, A., 2023. A comparison of $^{87}\text{Rb}/^{87}\text{Sr}$ and $^{40}\text{Ar}/^{39}\text{Ar}$
575 dates: Evaluating the problem of excess ^{40}Ar in Himalayan mica. *Earth and Planetary Science*
576 *Letters*, 609: 118058.
- 577 Laureijs, C.T., Coogan, L.A., Spence, J., 2021. In-situ Rb-Sr dating of celadonite from altered upper oceanic
578 crust using laser ablation ICP-MS/MS. *Chemical Geology*, 579.
- 579 Li, S.-S. et al., 2020. Coupled U-Pb and Rb-Sr laser ablation geochronology trace Archean to Proterozoic
580 crustal evolution in the Dharwar Craton, India. *Precambrian Research*, 343: 105709.
- 581 Li, Y., Vermeesch, P., 2021. Short communication: Inverse isochron regression for Re–Os, K–Ca and other
582 chronometers. *Geochronology*, 3(2): 415-420.
- 583 Liebmann, J., Kirkland, C.L., Kelsey, D.E., Korhonen, F.J., Rankenburg, K., 2022. Lithological fabric as a proxy
584 for Rb-Sr isotopic complexity. *Chemical Geology*, 608.



- 585 Longerich, H.P., Günther, D., Jackson, S.E., 1996. Elemental fractionation in laser ablation inductively
586 coupled plasma mass spectrometry. *Fresenius' Journal of Analytical Chemistry*, 355(5): 538-542.
- 587 Moens, L.J., Vanhaecke, F.F., Bandura, D.R., Baranov, V.I., Tanner, S.D., 2001. Elimination of isobaric
588 interferences in ICP-MS, using ion–molecule reaction chemistry: Rb/Sr age determination of
589 magmatic rocks, a case study. *Journal of Analytical Atomic Spectrometry*, 16(9): 991-994.
- 590 Mortimer, G.E., Cooper, J.A., James, P.R., 1987. U Pb and Rb Sr geochronology and geological
591 evolution of the Harts Range ruby mine area of the Arunta Inlier, central Australia. *Lithos*, 20(6):
592 445-467.
- 593 Norris, A., Danyushevsky, L., 2018. Towards Estimating the Complete Uncertainty Budget of Quantified
594 Results Measured By LA-ICP-MS. *Goldschmidt, Boston, USA (2018)*.
- 595 Olierook, H.K.H. et al., 2020. Resolving multiple geological events using in situ Rb–Sr geochronology:
596 implications for metallogenesis at Tropicana, Western Australia. *Geochronology*, 2(2): 283-303.
- 597 Phillips, G., Landenberger, B., Belousova, E.A., 2011. Building the New England Batholith, eastern
598 Australia—Linking granite petrogenesis with geodynamic setting using Hf isotopes in zircon.
599 *Lithos*, 122(1): 1-12.
- 600 Redaa, A. et al., 2023. Testing Nano-Powder and Fused-Glass Mineral Reference Materials for In Situ Rb-
601 Sr Dating of Glauconite, Phlogopite, Biotite and Feldspar via LA-ICP-MS/MS. *Geostandards and*
602 *Geoanalytical Research*, 47(1): 23-48.
- 603 Redaa, A. et al., 2021. Assessment of elemental fractionation and matrix effects during in situ Rb-Sr dating
604 of phlogopite by LA-ICP-MS/MS: implications for the accuracy and precision of mineral ages.
605 *Journal of Analytical Atomic Spectrometry*, 36(2): 322-344.
- 606 Roberts, N.M.W. et al., 2017. A calcite reference material for LA-ICP-MS U-Pb geochronology.
607 *Geochemistry, Geophysics, Geosystems*, 18(7): 2807-2814.
- 608 Rosel, D., Zack, T., 2022. LA-ICP-MS/MS Single-Spot Rb-Sr Dating. *Geostandards and Geoanalytical*
609 *Research*, 46(2): 143-168.
- 610 Rosenbaum, G., Li, P., Rubatto, D., 2012. The contorted New England Orogen (eastern Australia): New
611 evidence from U-Pb geochronology of early Permian granitoids. *Tectonics*, 31(1).
- 612 Sengun, F., Erlandsson, V.B., Hognmalm, J., Zack, T., 2019. In situ Rb-Sr dating of K-bearing minerals from
613 the orogenic Akcaabat gold deposit in the Menderes Massif, Western Anatolia, Turkey. *JOURNAL*
614 *OF ASIAN EARTH SCIENCES*, 185.
- 615 Shaw, S.E., Flood, R.H., 1981. The New England Batholith, eastern Australia: Geochemical variations in
616 time and space. *Journal of Geophysical Research: Solid Earth*, 86(B11): 10530-10544.
- 617 Simpson, A. et al., 2022. In situ Lu–Hf geochronology of calcite. *Geochronology*, 4(1): 353-372.
- 618 Tillberg, M. et al., 2021. Reconstructing craton-scale tectonic events via in situ Rb-Sr geochronology of
619 poly-phased vein mineralization. *Terra Nova*, 33(5): 502-510.
- 620 Tillberg, M. et al., 2020. In situ Rb-Sr dating of slickenfibres in deep crystalline basement faults. *Scientific*
621 *Reports*, 10(1).
- 622 Vermeesch, P., 2018. IsoplotR: A free and open toolbox for geochronology. *Geoscience Frontiers*, 9(5):
623 1479-1493.
- 624 Villa, I.M., De Bièvre, P., Holden, N.E., Renne, P.R., 2015. IUPAC-IUGS recommendation on the half life of
625 ⁸⁷Rb. *Geochimica et Cosmochimica Acta*, 164: 382-385.
- 626 Wang, C.Y. et al., 2022. Advances in in-situ Rb-Sr dating using LA-ICP-MS/MS: applications to igneous rocks
627 of all ages and to the identification of unrecognized metamorphic events. *Chemical Geology*, 610.
- 628 Woodhead, J.D., Hergt, J.M., 2001. Strontium, Neodymium and Lead Isotope Analyses of NIST Glass
629 Certified Reference Materials: SRM 610, 612, 614. *Geostandards Newsletter*, 25(2-3): 261-266.
- 630 Zack, T., Hognmalm, K.J., 2016. Laser ablation Rb/Sr dating by online chemical separation of Rb and Sr in an
631 oxygen-filled reaction cell. *Chemical Geology*, 437: 120-133.